NASA/TM—2006-214114 120–ISROMAC–11

Seal Investigations of an Active Clearance Control System Concept

Bruce M. Steinetz
Glenn Research Center, Cleveland, Ohio

Shawn Taylor
University of Toledo, Toledo, Ohio

Jay Oswald
J&J Technical Solutions, Cleveland, Ohio

Jonathan A. DeCastro
QSS Group, Inc., Cleveland, Ohio

February 2006

The NASA STI Program Office . . . in Profile

Since its founding, NASA has been dedicated to the advancement of aeronautics and space science. The NASA Scientific and Technical Information (STI) Program Office plays a key part in helping NASA maintain this important role.

The NASA STI Program Office is operated by Langley Research Center, the Lead Center for NASA's scientific and technical information. The NASA STI Program Office provides access to the NASA STI Database, the largest collection of aeronautical and space science STI in the world. The Program Office is also NASA's institutional mechanism for disseminating the results of its research and development activities. These results are published by NASA in the NASA STI Report Series, which includes the following report types:

- TECHNICAL PUBLICATION. Reports of completed research or a major significant phase of research that present the results of NASA programs and include extensive data or theoretical analysis. Includes compilations of significant scientific and technical data and information deemed to be of continuing reference value. NASA's counterpart of peer-reviewed formal professional papers but has less stringent limitations on manuscript length and extent of graphic presentations.

- TECHNICAL MEMORANDUM. Scientific and technical findings that are preliminary or of specialized interest, e.g., quick release reports, working papers, and bibliographies that contain minimal annotation. Does not contain extensive analysis.

- CONTRACTOR REPORT. Scientific and technical findings by NASA-sponsored contractors and grantees.

- CONFERENCE PUBLICATION. Collected papers from scientific and technical conferences, symposia, seminars, or other meetings sponsored or cosponsored by NASA.

- SPECIAL PUBLICATION. Scientific, technical, or historical information from NASA programs, projects, and missions, often concerned with subjects having substantial public interest.

- TECHNICAL TRANSLATION. English-language translations of foreign scientific and technical material pertinent to NASA's mission.

Specialized services that complement the STI Program Office's diverse offerings include creating custom thesauri, building customized databases, organizing and publishing research results . . . even providing videos.

For more information about the NASA STI Program Office, see the following:

- Access the NASA STI Program Home Page at ***http://www.sti.nasa.gov***

- E-mail your question via the Internet to help@sti.nasa.gov

- Fax your question to the NASA Access Help Desk at 301–621–0134

- Telephone the NASA Access Help Desk at 301–621–0390

- Write to:
  NASA Access Help Desk
  NASA Center for AeroSpace Information
  7121 Standard Drive
  Hanover, MD 21076

NASA/TM—2006-214114 120–ISROMAC–11

Seal Investigations of an Active Clearance Control System Concept

Bruce M. Steinetz
Glenn Research Center, Cleveland, Ohio

Shawn Taylor
University of Toledo, Toledo, Ohio

Jay Oswald
J&J Technical Solutions, Cleveland, Ohio

Jonathan A. DeCastro
QSS Group, Inc., Cleveland, Ohio

Prepared for the
11th International Symposium on Transport Phenomena
and Dynamics of Rotating Machinery
sponsored by the Pacific Center of Thermal Fluids Engineering
Honolulu, Hawaii, February 26–March 2, 2006

National Aeronautics and
Space Administration

Glenn Research Center

February 2006

Acknowledgments

The authors would like to acknowledge the support of NASA Glenn's Ultra-Efficient Engine Technology (UEET) projects: Intelligent Propulsion Systems and Foundation Technologies (IPSFT) and Propulsion 21 for their financial support. The authors also acknowledge the contributions of the following people: Scott Lattime, Malcolm Robbie, Art Erker, and Tobie Mintz for their design and fabrication support, and Richard Tashjian, Kevin McCormick, Tom Lawrence, Mike McGhee, and Joe Wisniewski for their technical assistance during the test rig installation and troubleshooting. Finally, the authors acknowledge Robert Hendricks for his thoughtful review of the manuscript.

Available from

NASA Center for Aerospace Information
7121 Standard Drive
Hanover, MD 21076

National Technical Information Service
5285 Port Royal Road
Springfield, VA 22100

Available electronically at http://gltrs.grc.nasa.gov

Seal Investigations of an Active Clearance Control System Concept

Bruce M. Steinetz
National Aeronautics and Space Administration
Glenn Research Center
Cleveland, Ohio 44135

Shawn Taylor
University of Toledo
Toledo, Ohio 43606

Jay Oswald
J&J Technical Solutions
Cleveland, Ohio 44130

Jonathan A. DeCastro
QSS Group, Inc.
Cleveland, Ohio 44135

Abstract

In an effort to improve upon current thermal active clearance control methods, a first generation, fast-acting mechanically actuated, active clearance control system has been designed and installed into a non-rotating test rig. In order to harvest the benefit of tighter blade tip clearances, low-leakage seals are required for the actuated carrier segments of the seal shroud to prevent excessive leakage of compressor discharge (P3) cooling air. The test rig was designed and fabricated to facilitate the evaluation of these types of seals, identify seal leakage sources, and test other active clearance control system concepts.

The objective of this paper is to present both experimental and analytical investigations into the nature of the face-seal to seal-carrier interface. Finite element analyses were used to examine face seal contact pressures and edge-loading under multiple loading conditions, varied E-seal positions and two new face seal heights. The analyses indicated that moving the E-seal inward radially and reducing face seal height would lead to more uniform contact conditions between the face seal and the carriers. Lab testing confirmed that moving the balance diameter inward radially caused a decrease in overall system leakage.

Introduction

Blade tip sealing has remained a challenging problem since the development of the gas turbine engine. Environmental conditions at the tip seal location include gas temperatures up to 2500 °F, pressures up to 500 psi, high surface speeds (1900 fps), as well as unburned jet fuel and contaminants (dirt, sand, etc.) that make for very challenging surroundings. Clearances change during engine operation as a result of both mechanical (pressure and rotational) and thermal loads.

Discrete structural mounts coupled with thermal and flight loads result in non-uniform distortions and asymmetric clearances. Designers of clearance control schemes must properly account for all of these effects to implement a successful active clearance control (ACC) system.

Improved blade-tip sealing in both the high pressure compressor (HPC) and high pressure turbine (HPT) can provide dramatic reductions in specific fuel consumption (SFC), lower emissions, increased compressor stall margin, and engine efficiency, as well as increased payload and mission range capabilities. Current clearance control systems employ scheduled cooling of the outer case flanges to reduce high pressure turbine tip clearances during cruise conditions. These systems have relatively slow response and do not use clearance measurement thereby limiting possible efficiency gains.

This paper describes work done to-date to evaluate a fast-acting, mechanically-actuated, active-clearance control concept with clearance measurement to help overcome some of the noted limitations.

Nomenclature

Flow Area	flow area (in^2) where flow is choked
Circumference	π×Diameter (in.)
$\dot{m}$	measured flow rate (lb_m/sec)
R	gas constant for air (53.3 lb_f-ft / lb_m-°R)
T	temperature (°R)
g_c	gravitational constant (32.2 lb_m-ft/lb_f-sec^2)
P_{supply}	supply pressure (psia)
h	face seal modified height
δ	radial movement of E-seal for figure 9b analysis
α	radial movement of E-seal for figure 9c analysis

Background

Figure 1 shows the high pressure HPT blade tip seal location in a modern gas turbine engine [1]. The figure shows a cross section of the combustor and two-stage HPT. The turbine disk, blade, and tip seal of the first-stage turbine are labeled. Blade tip or outer air seals line the inside of the stationary case forming a shroud around the rotating blades, limiting the gas that spills over the tips. Blade tip clearance varies both with engine operating points (e.g., ground idle, takeoff, cruise, decel, etc.) and cycle life. These clearance variations are due to a number of loads on both static and rotating parts and wear of these parts.

Load mechanisms can be separated into two categories, namely engine (power-induced) loads and flight loads. Engine loads include centrifugal, thermal, internal engine pressure, and thrust loads. Flight loads include inertial (gravitational), aerodynamic (external pressure), and gyroscopic loads. Engine loads can produce both axisymmetric and asymmetric clearance changes. Flight loads generally produce asymmetric clearance changes. Load mechanisms generally act to temporarily alter blade tip clearance. Wear mechanisms permanently change tip clearance. The ACC system must be designed to handle even the worst case transient conditions such as a stop-cock event where the engine is shutdown in-flight, allowed to windmill for a while, then restarted to full power.

The backside of the HPT shroud (blade outer-air-seal) is generally cooled with compressor discharge air (T3 air: 1200 to 1300 °F). This cooling is necessary for the shroud segments to survive the rotor inlet gas temperatures in excess of 2500 °F. The cooling air is also used to purge the leading and trailing edges of the shroud segments, providing a positive back-flow margin. This cooling flow is shown in figure 2 for the first stage shroud of a two-stage HPT. The pressures surrounding the shroud segment can be expressed as a function of the compressor discharge pressure (CDP; P3). Flow path pressure adjacent to the HPT shroud varies axially due to the work extracted by the turbine blades. For large commercial engines, the pressure of the cooling air behind the shroud is about 60 to 80 percent of P3 pressure [2]. Pressure in the tip clearance region varies axially from the leading to the trailing edge of the shroud about 70 to 30 percent of the P3, respectively. To maintain a positive backflow margin from the rotor inlet air, the cooling pressure on the backside of the shroud must always be higher than the rotor inlet side. The radial pressure difference across the shroud creates a load inward toward the shaft centerline. A resultant moment also exists on the shroud that is created by the non-uniform axial pressure distribution. P3

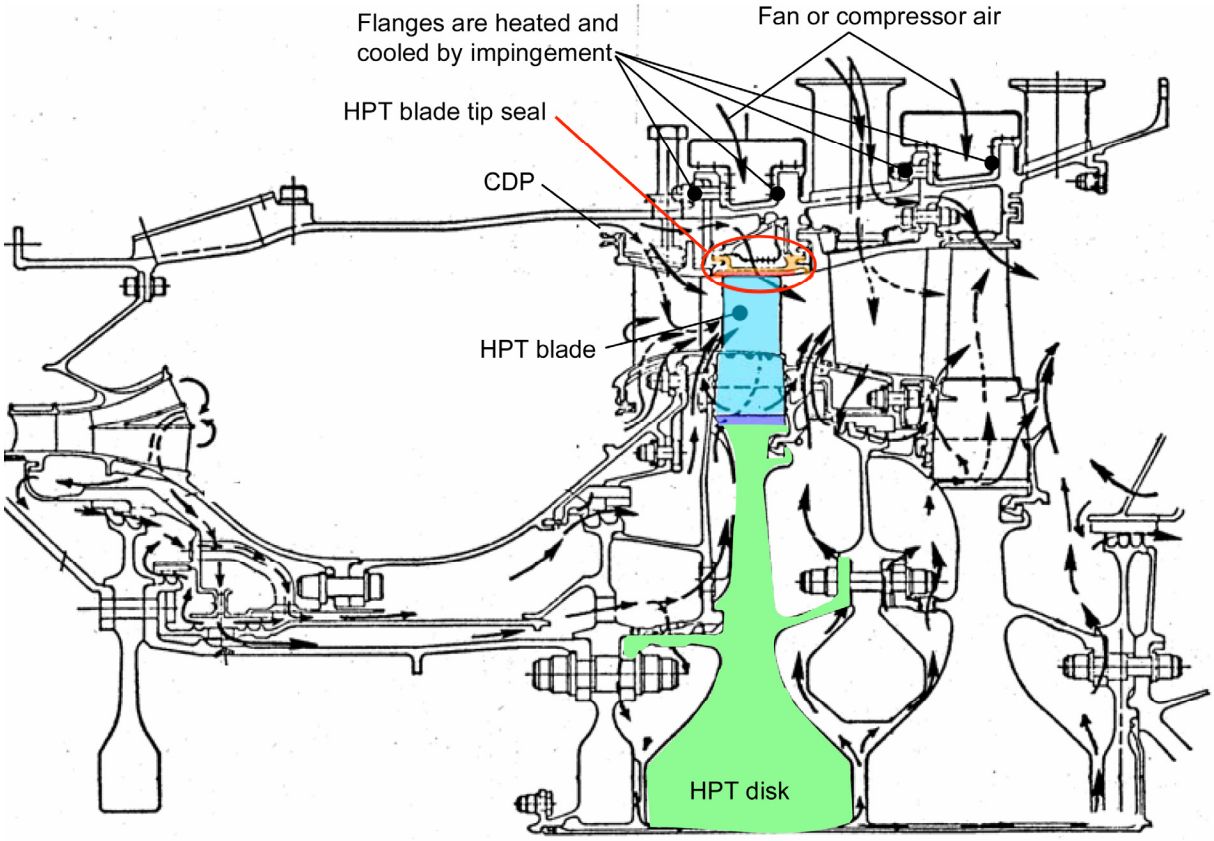

Figure 1.—HPT blade tip seal location in a modern gas turbine engine [1].

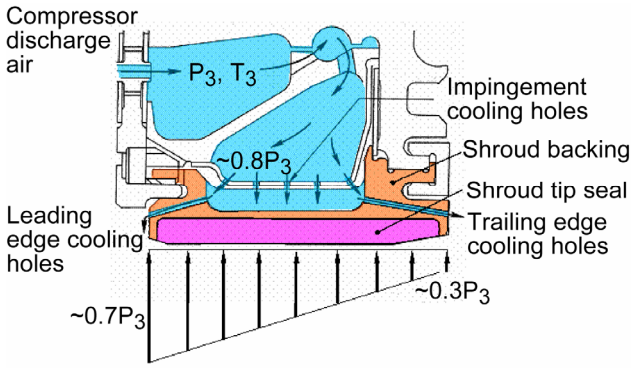

Figure 2.—Axial pressure distribution across HPT blade tip seal cross section [2].

pressure is highest during maximum thrust events such as takeoff and re-accel. For large commercial engines this translates to a maximum cooling air pressure differential of up to 150-psid across the shroud.

Lattime and Steinetz [2] provided a comprehensive review of the mechanisms of tip clearance variation, their effects in gas turbine engines, methods of controlling tip clearance and the benefits associated with reducing tip clearance. Kawecki [3] presented trade studies of a variety of approaches for active clearance control identifying a variety of fast-acting mechanical and novel thermal control systems. Melcher and Kypuros [4] outlined NASA Glenn's general approach for developing a fast-response ACC system and DeCastro and Melcher [5] examined the control systems requirements for fast acting ACC systems. Lattime et al. [6] designed a first generation, fast acting mechanical active clearance control system integrated into a test rig to evaluate its performance. Steinetz et al. [7] assessed leakage, positional accuracy, repeatability, and control of the fast-acting, mechanical active clearance control system. The current work builds on that initial investigation.

Benefits of Active Clearance Control

Blade tip clearance directly influences gas turbine performance, efficiency, and life. Reducing air leakage over the blade tips increases turbine efficiency and permits the engine to meet performance and thrust goals with less fuel burn and lower rotor inlet temperatures. Running the turbine at lower temperatures increases the cycle life of hot section components, which in turn, increases engine service life by increasing the time between overhauls.

Lattime and Steinetz [6], GE [8], and Wiseman and Guo [9] provide overviews of the many benefits of advanced active clearance control systems. Some of the more noteworthy benefits of implementing fast mechanical ACC systems in the HPT of a modern high bypass engine are provided herein for completeness. In terms of fuel savings, a tip clearance reduction of 0.010-in. results in ~0.8 to 1 percent decrease in specific fuel consumption. By reducing fuel burn significant reductions in NO_x, CO, and CO_2 emissions are also possible. Reducing tip clearances by 0.010-in. decreases exhaust gas temperature (EGT) ~10 °C. Deterioration of EGT margin is the primary reason for aircraft engine removal from service. Running the engine at lower operating temperatures can result in increased life of hot section components and extend engine time-on-wing (up to 1000 cycles). Additional benefits include increased payload and mission range capabilities.

Study Objectives

This work is part of a larger research effort to develop approaches for clearance control systems for use in the HPT section of large commercial aircraft engines to improve upon the case-cooling methods employed today. The objective of the current work is to present both experimental and analytical investigations into the nature of the face-seal to seal-carrier interface evaluated in the active clearance control test rig. Specific objectives of this study include:

- Experimentally examine whether the face-seal to seal-carrier interface can be improved to lower parasitic losses.
- Analytically determine the nature of the contact pressures between the face seal and the seal carriers for a variety of pressure differentials, E-seal positions, and seal carrier motion conditions.
- Analytically determine other candidate face seal designs to improve upon the baseline seal design.

Test Apparatus and Procedures

Apparatus

An active clearance control system test rig has been developed and installed (fig. 3). The key features of the test rig are summarized below. For a comprehensive review of the test rig design approach, the reader is directed to Lattime and Steinetz [6].

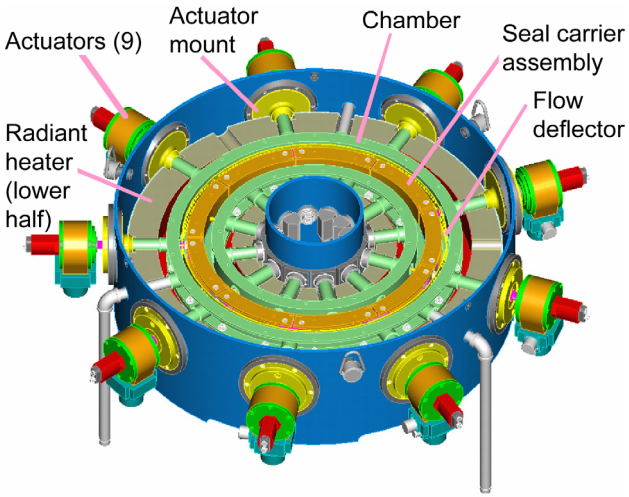

Figure 3.—ACC test rig with housing lid and chamber cover plate removed for clarity.

TABLE 1.—COMPARISON OF ACC RIG DESIGN AND A TYPICAL MODERN HIGH BYPASS RATIO ENGINE OPERATING CHARACTERISTICS

Parameter	ACC Rig Design	Reference Engine
Shroud backside pressure (psia)	135	500
Pressure differential (psid)	120	150
Shroud Backside temperature		
Current (°F)	1000	1250
Future (°F)	1250 to 1300	1250 to 1300
Diameter (in.)	20	30
Shroud face width (in.)	2	2
Number of shrouds/seal carriers	9	16
Pressure induced load on actuator (at pressure differential) (lbf)	1650	1750
Clearance change (e.g., stroke) (in.)	0.190	0.05 nom.
Clearance change rate (in./sec)	0.01	0.01
Clearance Measurement Technique		
Current	capacitance	not used
Future (under development)	microwave	capacitance/ microwave

General Overview

The ACC test rig simulates the environment surrounding the backsides of the turbine shroud segments. The purpose of the test rig is to evaluate actuation systems in a "static" environment without blade rotation. The rig design concentrated on simulating the temperature and pressure conditions that exist on the backsides of the seal segments, without the need for a rotating turbine, which greatly simplified the rig design. Rig specifications were chosen to closely simulate engine conditions. Table 1 compares the main characteristics of both the ACC test rig and a typical modern high bypass ratio engine.

The general features of the test rig are highlighted in figures 3 to 5. The rig main housing consists of two concentric cylinders, which form an annular cavity. A two-piece annular radiant heater (upper and lower halves) surrounds the seal test chamber to simulate the HPT tip seal backside temperature (T3) and pressure (P3) environment. At the heart of the rig is a segmented shroud structure (seal carrier) that would structurally support the tip seal shroud segments in an engine. Radial movement of the seal carriers controls the effective position/diameter of the seal shroud segments, thereby controlling blade tip clearance. The carrier segments are connected to one another through a pinned and slotted link as shown in figure 4. This link (or "foot") positions the carrier segments radially while allowing relative circumferential

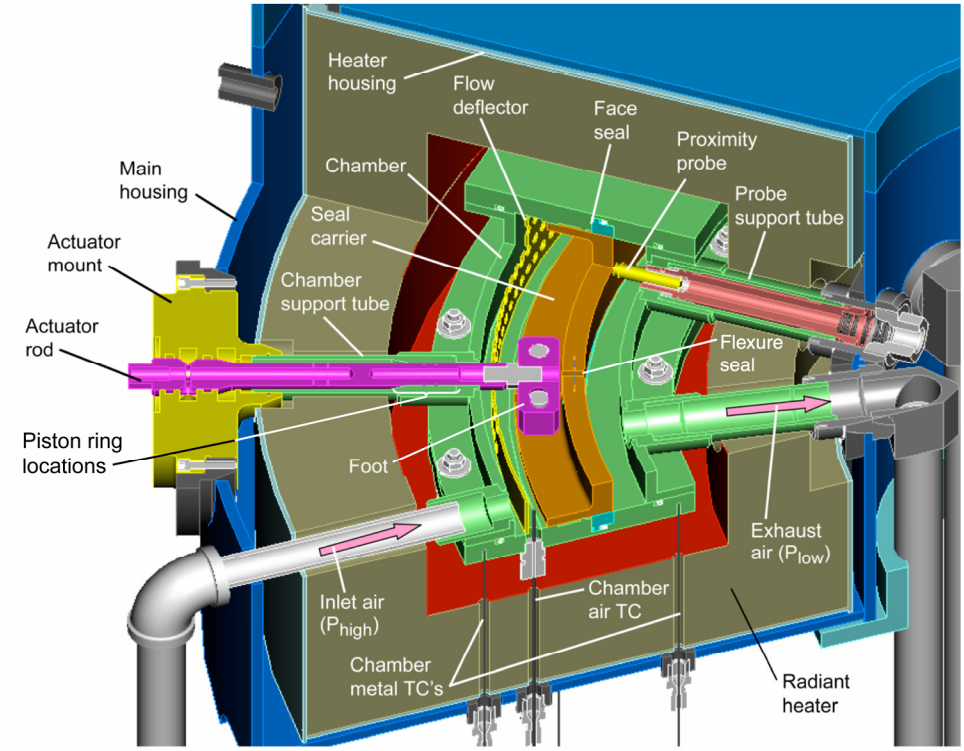

Figure 4.—ACC cut-away showing detail for one of nine actuator rods and attachment foot, actuator mount, seal carriers, proximity probe clearance sensor, inlet air supply pipe, air flow directions, and radiant heater [6].

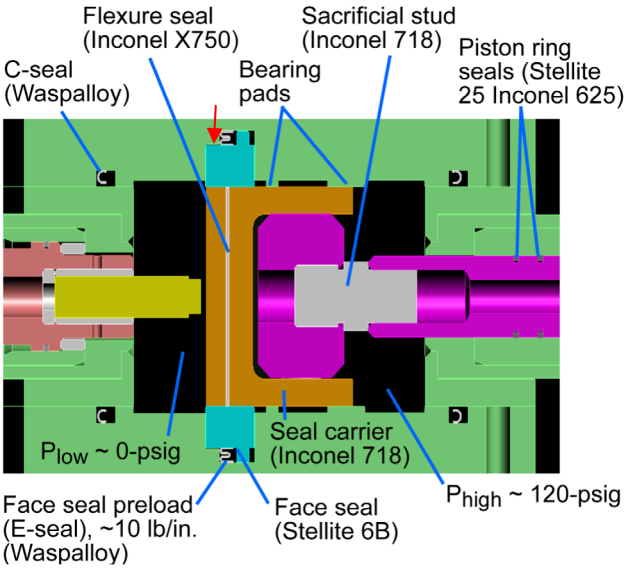

Figure 5.—Chamber detail showing seal carrier and adjacent face seals with E-seal preloader, actuator rod piston ring seals (2 places), chamber cover C-rings (4 places), the materials used in construction, and chamber high and low pressures. Red arrow indicates location of trial seal, as discussed in the Procedure Section.

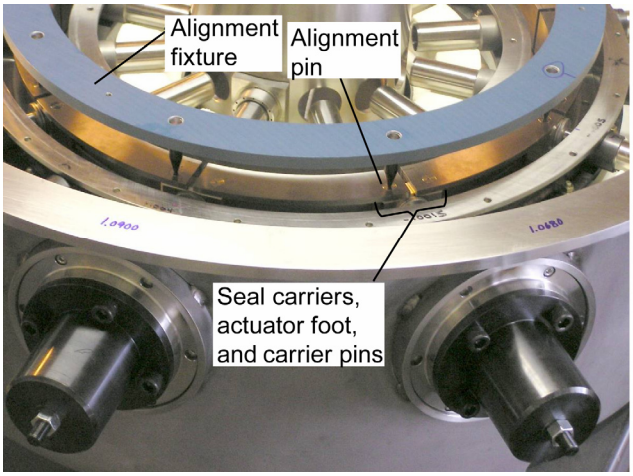

Figure 6.—ACC test rig with carrier alignment fixture installed. Note gage pins insert into precision centering holes in carrier pins. Alignment fixture used to set nominal or "home" position for all carrier segments.

movement or dilation of the seal carrier segments. A photograph of the test rig is shown in figure 6. Here the precision alignment fixture used to establish seal carrier concentricity relative to the rig centerline is installed. Tapered gage pins mounted in the alignment fixture engage precision alignment holes machined in the ends of the carrier pins. This alignment fixture or "gage plate" was used to define the nominal or "home" position for subsequent tests.

Chamber and Seal Detail

The pressurized test chamber encloses the carrier segments inside the annular heater through which pressurized air (heated for future tests) is supplied to simulate the P3 cooling/purge air pressure on the seal carrier backsides. The pressurized air is sealed along the sides of the seal carrier segments by contacting face seals that are energized via metal "E-seals" imbedded in the upper and lower chamber plates (figs. 4 and 5). The space between adjoining carrier segments is sealed with thin flexure seals otherwise known as spline seals (figs. 4 and 5). The face seal width was selected to seal the sliding interface between the edges of the flexure seals as they move radially inward/outward during actuation at moderately slow speeds (e.g., 0.01 in./sec). To minimize leakage, the face seal should always be in sealing contact with the edges of the flexure seals. The chamber penetrations for the nine actuator rods are sealed using two sets of concentric piston ring seals. A series of radial tubes projecting outward from the chamber's inner and outer side walls serve as supports, air supply and exhaust ports, probe mounts, and the actuator rod guides. These are sealed in their respective bosses via a shrink fit qualified through hydro-testing. The chamber functions to support and align the carrier segments and actuator rods, as well as to house instrumentation and to seal the pressurized air from the radiant heater which is not designed to carry any pressure loading. The chamber cover plates are sealed using inner- and outer-flange C-rings. Only the outer C-rings carry pressure during operation. The pipes supplying high pressure to the chamber (fig. 4) are also sealed using two sets of concentric piston ring seals.

Component Seal Leakage Evaluation.—The relative contribution of each seal component to the total system leakage was determined by Steinetz et al. [7]. The flexure seals contribute the majority of the leakage at 85 percent of the total. The face seals contribute the next highest percentage at 7 percent of total flow. The piston rings for the nine actuator rods contribute 6 percent. The rig supporting seals (e.g., air inlet piston rings and the four C-ring seals) contribute approximately 2 percent of the total.

Actuators and Position Measurement

Electric stepper motors were used to position the seal carriers for the current set of tests. Each stepper motor is equipped with a quadrature encoder to measure both shaft rotational position and direction of motion. A complete list of specifications is presented in Table 2. The stepper motors are rated for 500 lbf of actuation force. This limited the maximum chamber pressure that could be tested. Although calculations indicated that chamber pressures of 35 psig would result in 500 lbf actuator loads, actual tests indicated that the practical upper pressure was in the 20 to 30 psig range. It is expected that this noted difference is due to component friction. Stepper motors were selected as low-cost first generation actuators because of their high reliability and conduciveness to accurate position control. These actuators are therefore useful in evaluating the kinematics, seals, sensors, and control electronics under moderate loading conditions. Researchers are procuring a series of servo-hydraulic actuators designed to be able to handle the full 120 psig test pressure. These servo-hydraulic actuators will come equipped with linear

TABLE 2.—STEPPER MOTOR SPECIFICATIONS

Maximum load capability (lbf)	500
Stroke (in.)	0.5
Displacement resolution: without micro-stepping (in)	0.0005
Displacement resolution: with micro-stepping (in)	10 micro steps, 0.00005
Encoder resolution (in.)	0.000125
Voltage (V)	24
Current draw-peak (amps)	1.4 max
Weight (lbs)	5
Manufacturer	Haydon Switch and Instrument, Inc.
Model no.	87H43–12–002

TABLE 3.—INSTRUMENTATION SPECIFICATIONS

Thermocouples	Type K
Manufacturer	Omega
Accuracy (°F)	± 4
Range (°F)	–328 to 2282
Pressure Transducers	
Manufacturer	Druck
Model no.	PMP4010
Accuracy (psi)	0.12
Range (psi)	0 to 300
Flow meter	
Manufacturer	Teledyne-Hastings
Model no.	HFM-306
Accuracy (lbm/s)	0.0022 (1.2% full scale)
Range (lbm/s; SLPM)	0.19; 4000

TABLE 4.—CAPACITANCE CLEARANCE PROBE SPECIFICATIONS

Calibrated operating maximum temperature	1500 °F
Measurement range (in.)	0 to 0.125
Accuracy (in.)	0.0002
Resolution (in.)	0.00005
Excitation voltage (V)	15
Probe diameter (in.)	0.375
Stand-off distance for current tests (in.)	0.025
Weight (lbs)	0.04
Manufacturer	Capacitec
Model no.	HPC 150

variable differential transducers (LVDTs) to accurately measure actuator piston location.

Instrumentation

A variety of thermocouples, pressure transducers and flow meters were used to collect the necessary data. Table 3 provides a list of the transducer specifications and their respective accuracies. High temperature capacitance clearance probes were used to measure the radial displacement of the seal carriers (fig. 4) at three different circumferential locations for the mission simulated clearance tests performed in Steinetz et al. [7] and discussed in the Control Implementation section below. Table 4 provides a list of the probe specifications. Two capacitance clearance probes were mounted diametrally opposite one another and the third was clocked at 90° relative to the first two.

Data Acquisition System

A National Instruments (NI) LabVIEW-based program running on a PC host computer was used to implement data acquisition and stepper motor control. Temperature, pressure, and flow are measured at a rate of two samples per second, and position data (motor encoders and clearance probes) are sampled at 20 samples per second. The data is digitized with a 12 bit analog/digital (A/D) card. The stepper motors are controlled with two 8 axes motion control cards located in a remote chassis. Communication delays between the PC and the chassis limits the control loop time to approximately 50 ms.

Control Implementation

The active clearance control system was implemented in NI LabVIEW with an NI motion control blockset that allows the nine stepper motors to be controlled simultaneously via motion control cards. The advantage of using motion control is that stepper motor "positional moves" commanded by LabVIEW are generated by the motion control cards and hence operate independently of the software (limited to 50 ms updates). When LabVIEW commands a "positional move," a desired position and velocity is fed to the motion control board and the move begins.

The actuators were controlled in either open-loop or closed-loop modes. For the leakage vs. carrier position tests performed herein, the actuators were controlled in open-loop mode. In open-loop mode, a single position move was commanded to all nine actuators. Motion stops after the commanded number of motor steps have been executed.

As described in Steinetz et al. [7], closed loop control was used for evaluating the ability of the ACC system to maintain a tight clearance set-point during simulated engine transients. An on-off set point tracking controller was implemented in LabVIEW to track simulated clearance transients with the stepper motor actuators. An error signal was computed every 50 ms by subtracting the actual clearance (as measured by the proximity probes) from the desired clearance set-point. A position move equal to the magnitude and direction of the error signal was commanded to the stepper motors. If the move completed before 50 ms elapses, then the motor would stop until the next cycle began. If the move did not complete, the motor would remain in motion, but, with updated commands. In order to minimize tracking delays due to error propagation, the motor velocity was set to a value of 0.010 in./sec.

Simulated Engine Clearance versus Time Study.— Steinetz et al. [7] examined the closed-loop positional accuracy for the ACC system while simulating an engine clearance versus time study. Figure 7 shows the results of those tests here for completeness. The set-point position defines ideal carrier position movement versus time for a simulated take-off

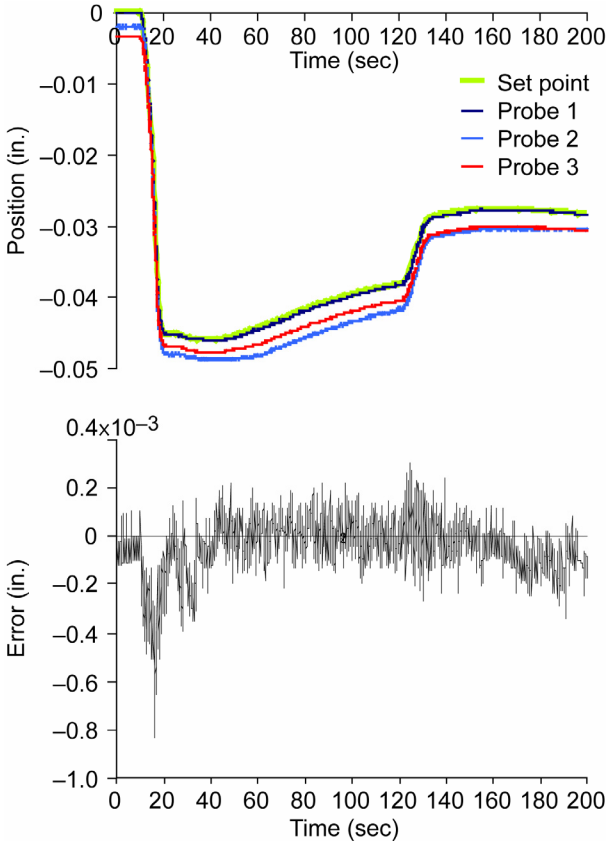

Figure 7.—ACC test rig simulation of engine clearance transient during take-off conditions. (a) Commanded (e.g., set point) and measured carrier position (using capacitance probes). Negative position indicates movement radially outward from start position or simulated "flight idle" condition; (b) Positional error versus time. Conditions: pressure 20 psig, ambient temperature, control based on minimum clearance of 3 capacitance probes [Steinetz et al. [7]].

condition (clearance change of 0.045 in.). These tests were performed at a pressure of 20 psig. Figure 7(a) shows the set-point and the measured carrier position at three clock positions: probe 1(0°), probe 2 (90°), probe 3 (180°). Throughout these tests the controller examined all three probes and controlled to the minimum clearance which in this case was at probe 1. Though it may difficult to see, the motion of the carrier adjacent probe 1 tracked the set-point very well. The carriers adjacent the other two probes were slightly further away from the probes from assembly set-up and those carriers remained further outward radially throughout the test.

Figure 7(b) shows the error defined as "set-point minus actual position" on a highly refined vertical scale. (Note that for this chart, negative error indicates the actuator did not move outward radially as far as the set-point). For the entire simulated take-off transient, the error between the set-point (green line) and probe data (black line) was less than 0.001-in. This was a very encouraging result as it showed that the kinematic system could track simulated engine clearance changes at the correct rate and range under load with an acceptable error. Note: Tests were also performed at chamber pressures of 10 and 30 psig. The results were generally the same except that the error tracked with pressure. This is the expected result as the higher pressure load (e.g., 30 psig) and corresponding frictional effects were just above what the stepper motor could reliably actuate without slowing down. Future hydraulic actuators are designed to eliminate this shortcoming.

Procedures: Experimental

Face Seal Contact

During the testing reported in Steinetz et al. [7], it was noticed that minor scuffing indications were present on the seal carriers near the outer diameter of the face seal. Contact at that location could indicate a flow path that was not fully considered in that study. If the contact between the face seal and the seal carriers was away from the edges of the flexure seals (e.g., face seal contact not coincident with the edges of the flexure seals), then leakage could travel inward radially past the face seals and exit over the top of the flexure seals through a wedge-shaped gap formed between the face seal and the seal carriers. Tests were performed herein to examine the nature of the face seal contact using pressure sensitive film. This pressure sensitive film is placed between two mating surfaces and exhibits a color change with color density proportional to the unit contact pressure. The pressure sensitive film used in the current study was obtained from Sensor Products Inc., East Hannover, NJ. Two contact pressure ranges were used in this study including the micro range (2 to 20 psi, black in color) and ultra low (range 28 to 85 psi, pink in color).

Face seal in contact with granite base.—A test was conducted to determine the uniformity of the contact pressure of the face seal in contact with a precision flat granite base. In this test, the face seal was loaded against the granite base with the ultra-low range pressure film positioned in 90° increments. The film width was approximately 1 in. The seal was then loaded with a bar placed across the center using gauge pins so as to load the center of the face seal. The bar was then loaded with approximately 200 lbf. For reference purposes, the face seal flatness specification was 0.0003 in. and roughness was 8 μin.

Face seal installed against seal carriers in test rig.—Pressure sensitive film was installed between the seal carriers and the face seal at six locations around the circumference of the face seal. Both the ultra low range film (~0.005 in. thick), and the micro range carbon paper based film (~0.012 in. thick) were used. The film types were alternated on a 60° angular pattern, leaving 120° between similar film types. The rig was built up with the E-seals in place behind the face seal. Air pressure was not applied. The test goal was to determine the face seal contact loading pattern when assembled. The bolts were tightened to 70 in.-lb, as typical for a room temperature build-up. For reference purposes, the seal carriers were made to the following specifications: flat to within 0.0003 in., opposite carrier faces parallel to 0.0005 in., and surface roughness of 10 μin.

Effect of Carrier Position on Leakage

Low ACC parasitic leakage is required in order to minimize P3 cooling air loss and to net the engine efficiency

gains from the tighter tip clearance. To quantify the ACC system leakage and possible improvements, two different static flow test setups were used.

Baseline Configuration.—In the baseline configuration, E-seals were assembled in their normal locations behind the face seals. Flow measurements were made with the following test conditions. Air or "engine" pressure was ramped from 10 psig up to 109 psig. For each of these pressures, the seal carriers were positioned at a variety of carrier positions ranging from 0.02 in. radially inward through home (e.g., 0.00 in.), to 0.08 in. radially outward, as indicated by the capacitance probes. During carrier movement, the air pressure was removed.

Trial Seal Configuration.—To evaluate the theory that increasing the engine pressure behind the face seal (e.g., changing the balance diameter) could better seat the face seal against the seal carriers and flexure seal, the upper E-seal was removed from the rig, and a circle of monofilament line (0.015 in. diam.) was installed at the mid-point of the land between the cover plate and the E-seal as indicated with the red arrow in figure 5 (radial dimension from face-seal centerline of 10.4 in.). The monofilament would act as both a seal and as a preloader. Vacuum grease was used to hold the monofilament line in place and a lap joint was used at the ends of the line to form a continuous loop around the back side of the face seal. Flow measurements were made using the same test conditions of air pressure and carrier position as described above.

Procedures: Analytical

Finite Element Model

To further understand the source of edge loading observed between the outer diameter of the face-seal and the seal-carriers, a series of finite element analyses were performed using ANSYS V9.0. In these analyses, the cover plate, the face seal, and the inner/outer chamber walls were modeled using axisymmetric elements. The elements used were 2-D, six-node, triangular structural solid elements (ANSYS: PLANE2). The contact surface of the face seal was modeled with 2-D, three-node, surface-to-surface contact elements (ANSYS: CONTA172). The carrier segments were modeled as rigid contact targets (ANSYS: TARGE169). Symmetry was invoked and only the upper face-seal to seal-carrier surface was analyzed. The cover plate was modeled to determine whether an interaction between the cover plate and the face seal could be affecting the face seal contact. Contact was not observed between the cover plate and the face seal during any of the finite element analyses. The seal carriers were assumed to be rigid. This assumption was followed as the seal carriers have air pressure on both their outer and inner surfaces minimizing the potential for bending of the seal carrier walls adjacent to the face seal. The face seal was modeled to evaluate what role the E-seal location (e.g., balance diameter), friction forces, and direction of motion might be playing in the observed face seal edge loading. The finite element analysis was also used to investigate alternate face seal designs.

Dimensions, Loads, and Boundary Conditions.—The relevant face seal dimensions used for the analyses are shown in figure 8. A summary of the different analysis cases examined are shown in figure 9. Face seal geometries modeled included: (a) baseline or as-built; (b) E-seal moved inward radially either

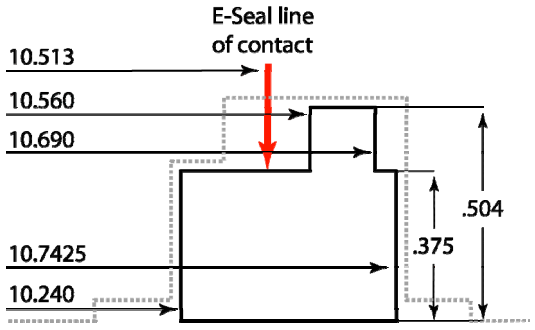

Figure 8.—Relevant face seal dimensions (in.) for analysis. E-seal baseline radius is 10.513 in. Note all dimensions emanating from left are radii. Phantom lines denote cover plate groove for reference.

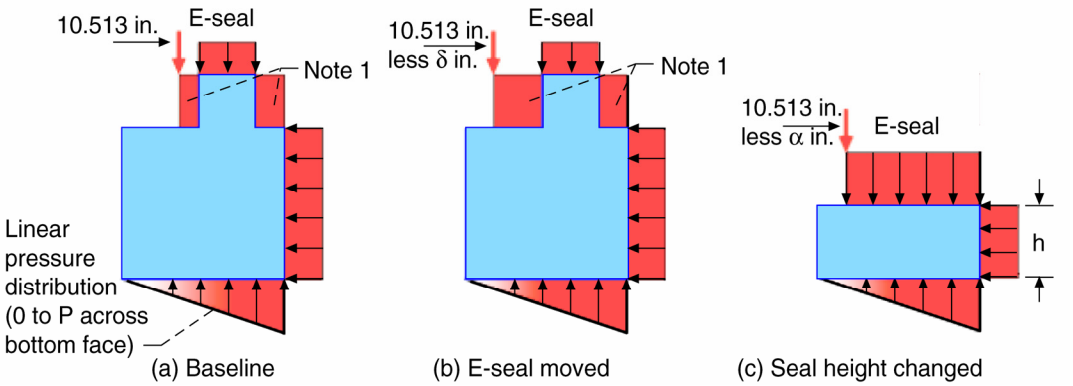

Note 1: Pressure loads (P) in both vertical and horizontal directions.

Figure 9.—Face seal geometries and air pressure loads (P) modeled. (a) Baseline; (b) E-seal moved inward radially (δ) either 0.1 or 0.2 in. relative to baseline, and (c) overall face seal height (h) reduced to either 0.25 and 0.1 in., with associated E-seal movement (α).

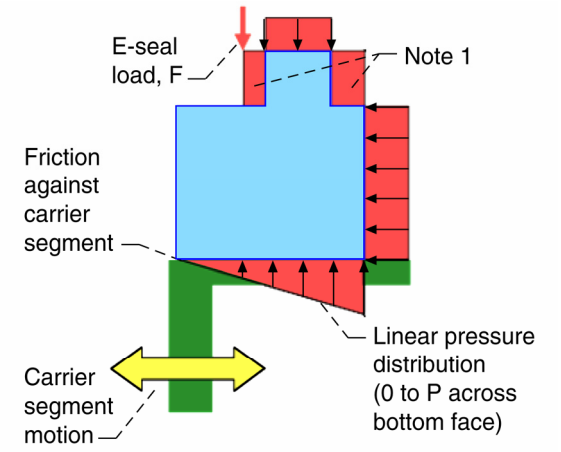

Note 1: Pressure loads (P) in both vertical and horizonal directions.

Figure 10.—Summary of load cases modeled for each geometry. Cases examined: Carrier segment motion: no motion, inward and outward motion; pressure loads (P), 30, 60, 120 psig; E-seal preload (F) 12 lbf/ circumferential inch; coefficient of friction = 0.3, contact load determined analytically using contact elements.

0.1 or 0.2 in. relative to baseline, (c) overall face seal height reduced to either 0.25 or 0.1 in., with associated E-seal movement (α) relative to baseline. Figure 10 summarizes the load boundary conditions and load cases modeled. Three carrier segment motions were considered: no carrier motion, inward motion, and outward motion. Applied air pressures considered included 30, 60, and 120 psig. A linear pressure distribution was used across the face of the face seal (0 to maximum air pressure). Air pressure was applied vertically and horizontally on other wetted surfaces up to the point of the E-seal to face seal contact. The E-seal preload (F) was held constant at 12 lbf/circumferential inch. The coefficient of friction between the face seal and the carrier was assumed to be 0.3. Coulomb friction was used therefore friction forces always resisted motion.

Grid refinement study.—A grid refinement study was performed to assess the effect of grid size on contact pressure solutions. In this study the element size was reduced in size by more than half in the interior of the face seal and reduced by a factor of 4 along the frictional interface.

Results and Discussion

Experimental Results

Face Seal Contact

Figures 11 and 12 show the results of the tests performed using pressure sensitive film to investigate the face seal contact pressure profile. Tests performed with the face seal against the precision flat granite base (fig. 11), showed uniform pressure across the seal face (inner to outer diameter), suggesting that the face seal was not deformed. Tests performed with the

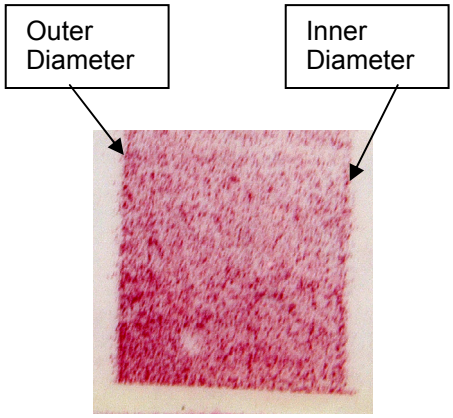

Figure 11.—Close-up of one of the pressure sensitive films used to characterize face- seal to granite-base contact pattern showing near uniform contact pressure across the face.

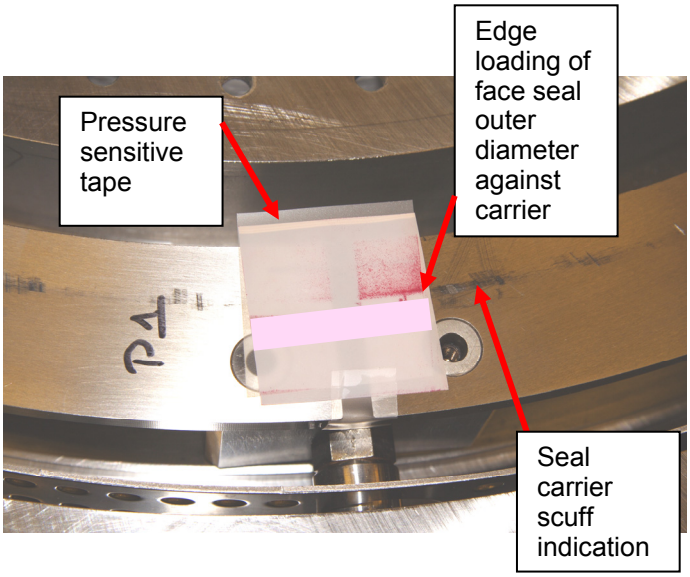

Figure 12.—Photo of test rig with chamber cover removed showing pressure sensitive film documenting face-seal to seal-carrier contact pressure for two neighboring carrier segments. Observations: the left hand seal carrier is less in contact with the face seal than the right hand carrier. Both carriers show higher contact pressures near the face seal outer diameter and lower contact pressures near face seal inner diameter.

pressure sensitive film between the face seal and the seal carriers showed two interesting findings, as shown in fig. 12. In this figure the film is laid across two adjacent seal carriers. The left carrier did not develop the film as much as the right hand carrier when preloaded using the E-seal. However in both cases the face seal exhibited edge-loading near the outer diameter of the face seal where it contacts the seal carriers. The line of load concentration fell on the centerline of the scuff marks

on the seal carriers, which was expected. This proved that the scuffing was likely an artifact of the uneven load pattern between the face seal and the seal carriers. A similar test was performed with the pressure-sensitive film as above but in addition to the preload from the E-seal, air pressure was applied. This test did not provide any conclusive results.

Effect of Seal Carrier Position on ACC Leakage

Figure 13 shows the result of the static leakage versus seal carrier position tests at a chamber pressure of 109 psig for the two build configurations: E-seal baseline and monofilament trial seal installed in place of the E-seal in the top cover plate location. Flow data is shown only for the high pressure differential where the greatest leakage vs. carrier position trend was observed.

E-Seal Baseline.—Relative to the home position, the system leakage was 0.052lbm/s lower when the carriers were moved 0.080 in. radially outward. This corresponds to a leakage reduction of about 50 percent, indicating that a considerable amount of flow is leaking through the face-seal to seal-carrier interface. It is believed that this leakage is greatest at the three-way intersection between the face seal, seal carriers and flexure seals. Leakage reductions were expected because as the seal carriers were moved outward, the face-seal to seal-carrier contact zone (e.g., scuffing area) better aligned with the diameter of the flexure seals.

Monofilament Trial Seal.—Relative to the home position, the system leakage was 0.027 lbm/s lower when the carriers were moved 0.080 in. radially outward. This corresponds to a leakage reduction of about 29 percent.

Comparison of Configurations.—Comparing leakage results, a couple of observations are made. First the overall leakage of the monofilament seal build is about 13 percent (0.014 lbm/s) lower than the E-seal build's leakage at the "home" or nominal position (e.g., carrier position = 0.00 in.). Furthermore the E-seal build leakage vs. carrier position curve is steeper than that of the monofilament in the 0.08 in. outward-to-home range. Comparing slopes, the E-seal build leakage vs.

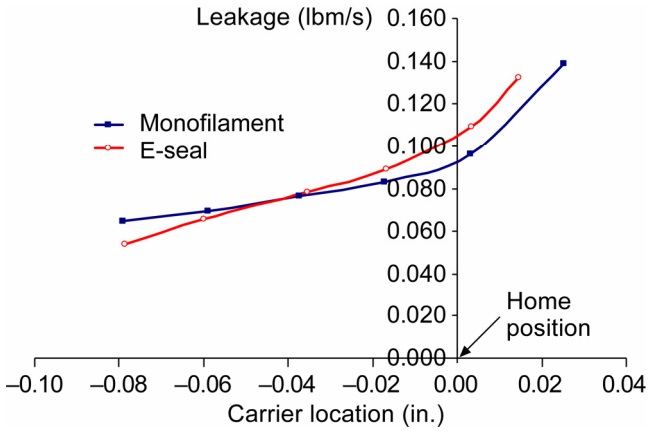

Figure 13.—Leakage versus actual seal carrier position for 109 psig pressure differential and two face seal backside configurations: Metal E-seal and monofilament trial seal.

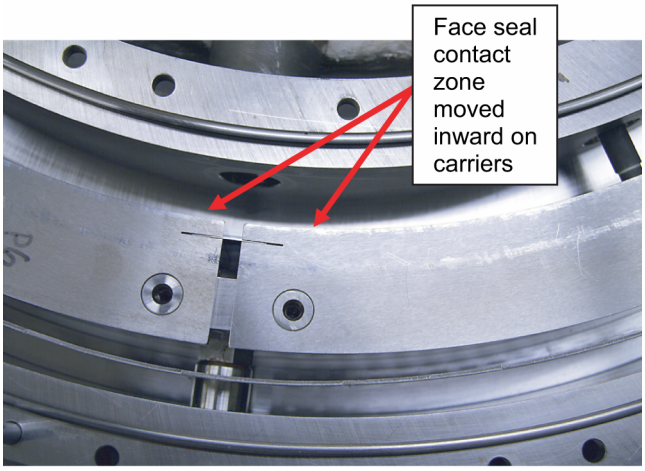

Figure 14.—Photo of two adjacent seal carriers and flexure seal showing face seal contact zone (minor scuffing marks) shifted near the inner diameter of the seal carriers. E-seal replaced with trial seal: monofilament behind the face seal.

carrier position slope is almost twice (1.85:1) that of the monofilament build. This is an interesting finding in that one recalls that only the upper E-seal was replaced with the monofilament trial seal. One might speculate that the slope of the monofilament trial seal build might be flatter should both upper and lower E-seals be replaced with monofilament trial seals. From an optimal design view point, a relatively flat leakage versus carrier position is desired. This condition would indicate seal leakage is insensitive to seal carrier position. In summary, the trial seal positioned such that engine pressure was exerted over a greater face-seal back-side surface area reduced the seal leakage and reduced the sensitivity of leakage to seal carrier location.

Figure 14 is a photograph of the hardware taken after the monofilament trial seal was tested in place of the E-seal. The photo shows two adjacent seal carriers and flexure seal showing the face seal contact zone (minor scuffing marks) shifted near the inner diameter of the seal carriers. It appears that changing the balance on the face seal is an effective way to improve sealing performance.

Comparison of Effective Seal Flow Area to Industry Reference Level

As stated earlier, low ACC parasitic losses are required to harvest the engine efficiency gains from the tighter tip clearance control. In the current section, a comparison of the measured losses in terms of effective leakage flow area per inch of circumference is made to an engine industry reference level.

Using the total measured leakage rates of all seal locations, an effective leakage flow area for the entire active clearance control system was back-calculated to compare to an engine industry reference level. The method used to back-calculate the effective leakage flow area was taken from an isentropic flow condition with compressibility at the choked-flow condition [10]. The leakage flow was considered choked since

the pressure ratio of 8.4 (i.e., $P_{supply}/P_{exhaust}$ = 123.7 psia/14.7 psia) was above the critical pressure ratio for air. The equation used was:

$$\frac{Flow\ Area}{Circumference} = \frac{\dot{m} \times \sqrt{R \times T}}{0.6847 \times \sqrt{g_c} \times P_{supply} \times Circumference}$$

where:

Flow Area	flow area (in^2) where flow is choked
Circumference	π×Diameter (in.)
$\dot{m}$	measured flow rate (lb_m/sec)
R	gas constant for air (53.3 lb_f-ft / lb_m-°R)
T	temperature (°R)
g_c	gravitational constant (32.2 lb_m-ft/lb_f-sec^2)
P_{supply}	supply pressure (psia)

Industry Reference Effective Flow Area.—If one were to idealize the ACC system as an elastic structure (e.g., rubber band) that could move radially inward/outward, seals would only be required between the sides of the seal carriers and the static structure. Engine designers have acknowledged that flows in these areas less than ~0.1 percent core-flow (W25) would be an acceptable loss considering the potential for the significant gains possible through the tighter HPT tip clearances. Converting this level into an effective flow area per unit circumference results in approximately 0.00048 in^2/in. of circumference. Since there are two seal locations the total effective flow area per unit of circumference would be twice the above or 0.00096 in^2/in. Figure 15 compares the effective flow area per unit circumference found experimentally for the two build conditions (E-seal and monofilament trial seal at the carrier "home" position) to this industry reference level. Though this current data is only for ambient conditions, the effective flow area for the ACC rig falls within the industry reference level.

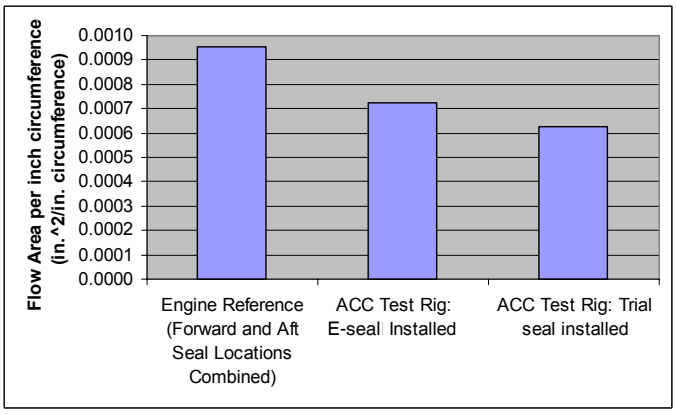

Figure 15.—ACC test rig effective flow area per inch circumference (back-calculated from leakage flow data) compared to engine reference flow area per inch circumference (for forward and aft seal locations). Seal carriers at "home" position for two builds: E-seal and monofilament trial seal.

Analytical Results

Baseline Face Seal Design

Figure 16 shows the results of the finite element analyses performed for the baseline face seal design with the E-seal positioned at the as-built location. Calculated contact pressures (in psi) are shown for three conditions: (a) no carrier motion, (b) carrier moving inward, (c) carrier moving outward. These studies were performed to assess whether either pressure loading or friction were contributing to the edge loading between the outer diameter of the face seal and the seal carriers. The results do indicate that pressure does play a role in edge-loading the face seal, as indicated for the 120 psig air pressure for all cases, and for pressures ≥ 30 psig air pressure when the carrier is moving inward. These edge loading results were corroborated by the experimental observations presented above. In the case where the carrier is moving inward, the contact friction tends to rotate the seal and causes edge loading, even at the lowest pressures (e.g., 30 psig).

Color plot scaling.—The reader is alerted that though all contact pressure results are plotted on the same scale, ANSYS scales the image to fill the ordinate space. Hence, note that on select plots the contact pressure is low (e.g., <28 psi) but it is still scaled to fill the ordinate space.

E-Seal Position Study

Figure 17 shows the calculated results of the face seal contact pressures for the baseline face seal configuration (e.g., original height) but with the E-seal analytically moved to two positions: 0.1 and 0.2 in. radially inward from baseline, for three conditions all at 120 psig engine pressure: (a) no carrier motion, (b) carrier moving inward, and (c) carrier moving outward. Of the two cases examined, positioning the face seal contact in 0.1 in. resulted in a fairly uniform contact stress for each of the three motion cases considered. Positioning the E-seal inward 0.2 in. caused relatively high edge loading (contact pressures up to 200 psi) on the inner diameter for the no-motion and carrier moving outward cases. Positioning of the E-seal requires careful balance to minimize face seal leakage while not causing excessive edge-loading for wear considerations.

Face Seal Height Study

Thinner face seals were considered in this study for two reasons. Thinner face seals present smaller areas over which the air pressures can act, which can mitigate the combined pressure/friction rotational moments that can occur on the seals. These moments can amplify edge-loading effects. Thinner face seals also are more flexible which may allow the face seals to more easily conform and seal to adjacent seal-carrier to seal-carrier out-of-plane movements.

Figure 18 shows the calculated contact pressures (in psi) for two reduced height face seals: 0.25 and 0.1 in. thick. In these cases, the E-seal was positioned inward 0.05 and 0.1 in. relative to the baseline, respectively. These E-seal positions were chosen for better contact pressure distribution. The results shown are for 120 psig engine pressure for three conditions: (a) no carrier motion, (b) carrier moving inward, and (c) carrier moving outward. The 0.25 in. face seal exhibited the lower overall contact stress and did not show edge loading.

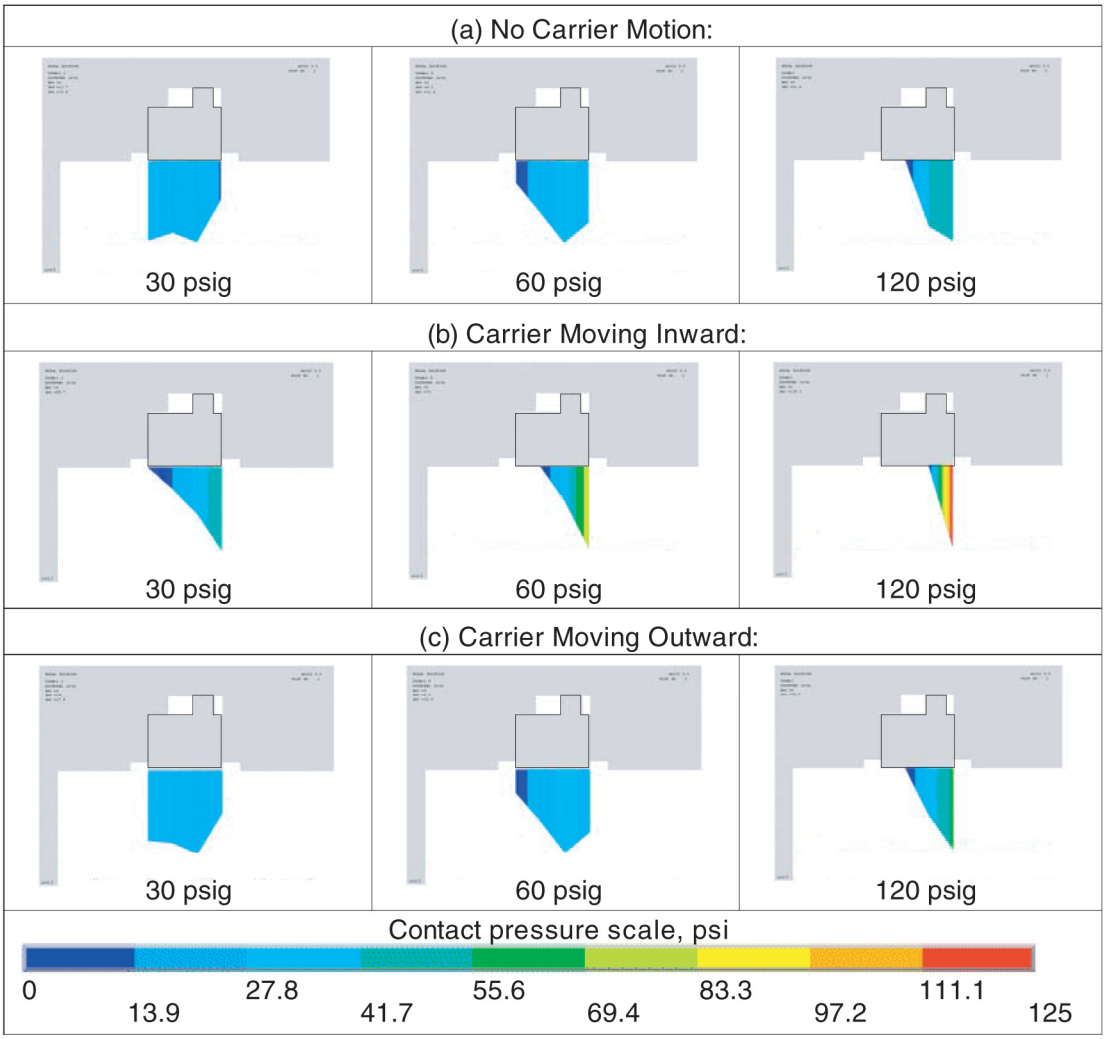

Figure 16.—Calculated contact pressures (in psi) for baseline face seal configuration with E-seal positioned as-built for three conditions: (a) no carrier motion, (b) carrier moving inward, (c) carrier moving outward.

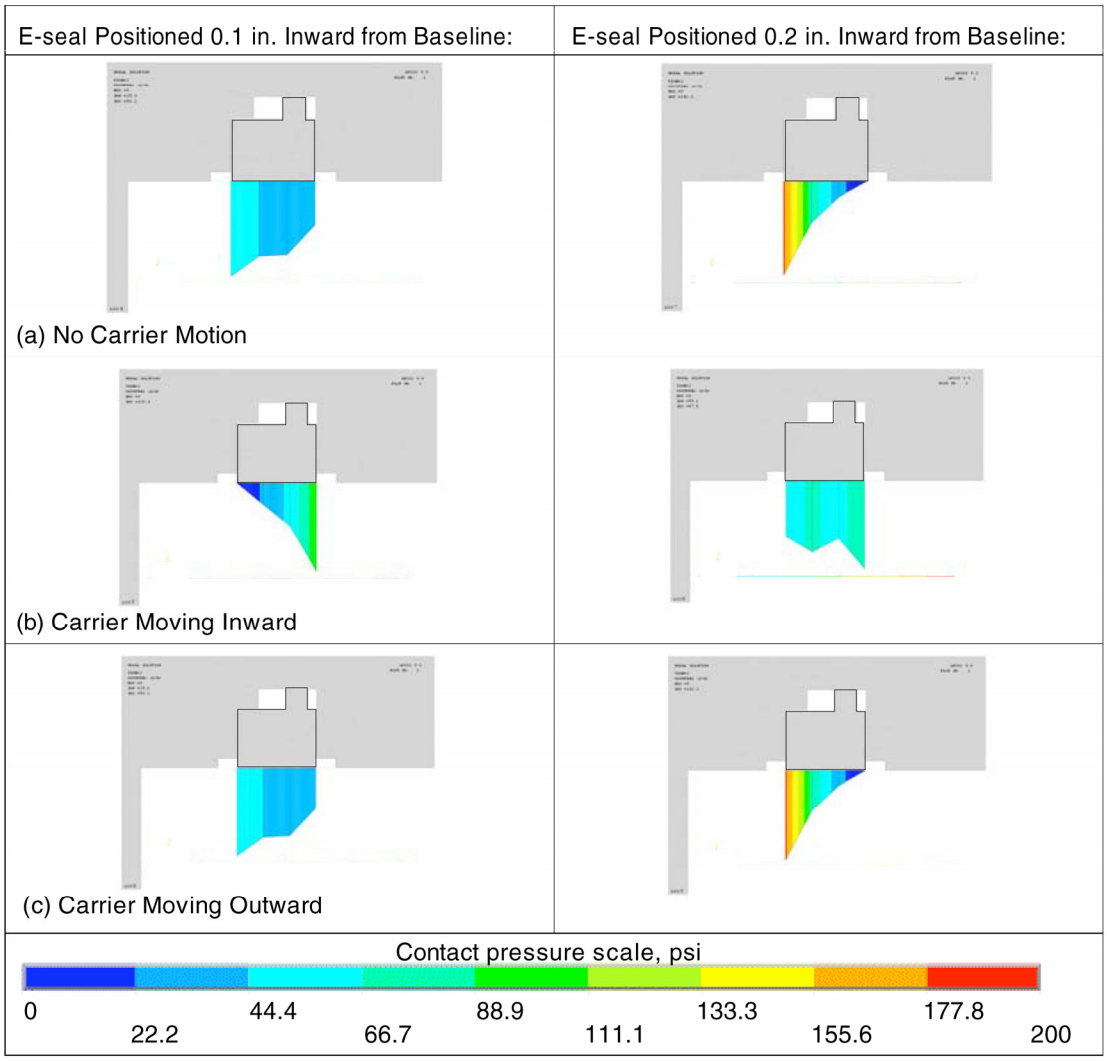

Figure 17.— Calculated contact pressures (in psi) for baseline face seal configuration but with E-seal analytically positioned to two different positions: 0.1 in. in radially inward and 0.2 in. from baseline, for three conditions all at 120 psig engine pressure: (a) no carrier motion, (b) carrier moving inward, (c) carrier moving outward.

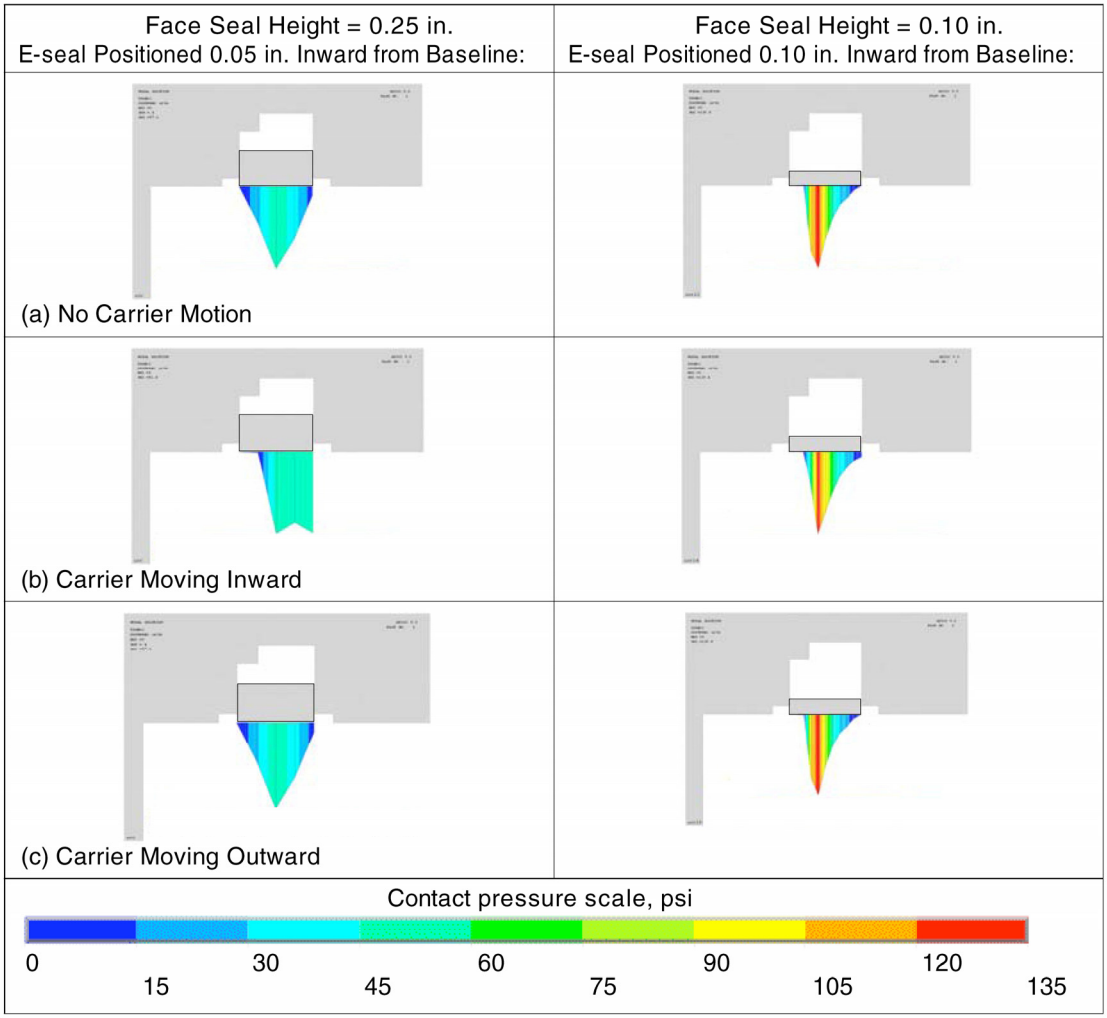

Figure 18.—Calculated contact pressures (in psi) for two reduced height face seals: 0.25 and 0.1 in. thick. E-seal positioned inward radially as indicated for best pressure distribution, all at 120 psig engine pressure for three conditions: (a) no carrier motion, (b) carrier moving inward, (c) carrier moving outward.

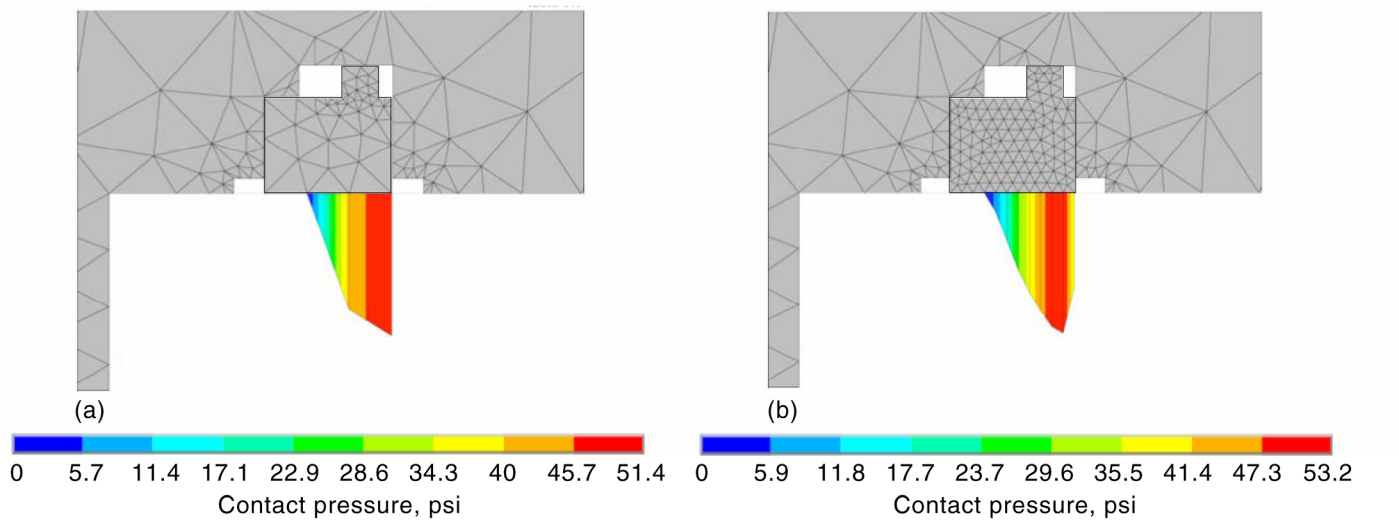

Figure 19.—Results of grid refinement study. (a) Baseline grid used to run analysis cases. (b) Refined mesh with 4 times the elements along the frictional contact surface. Note peak contact pressure (in psi) changed less than 4 percent.

Furthermore it was the least sensitive to the motion cases considered. The 0.10 in. face seal design did not show any edge loading. However it did exhibit higher contact stresses in the center, presumably because the thinner seal was more flexible. The features of these designs make them attractive for further experimental study.

Grid Refinement Study

The first case, (default geometry, no carrier motion, 120 psig pressure), was modeled with different face seal element sizes to determine whether or not the mesh was sufficiently refined. Figure 19 shows that the contact pressure changed less than 4 percent with the higher element density mesh. Therefore it was determined that the default element mesh was acceptable.

Summary and Conclusions

An active clearance control system concept and associated test rig has been fabricated and installed. The system is being used to evaluate different kinematic, seal, actuator, controller, and clearance-sensor approaches to achieve a fast-acting, mechanical active clearance control system to allow tighter turbine tip clearances in future turbine engines. The current study experimentally investigated the contact pressure distribution between the face seal and the carrier segments and the effects of carrier position on ACC system leakage rates. The current study investigated the system performance at appropriate pressure differentials but at ambient temperature. Future studies will examine performance under engine simulated pressures and temperatures.

The current study also analytically investigated, via finite element contact analyses, the effects of face-seal to seal-carrier contact pressure and edge-loading under several loading conditions, several positions or balance diameters of the E-seal, and two proposed face seal heights.

Based on the investigations performed herein, the following observations are made:

- Positioning the seal carriers such that the face seal contact zone was nearly coincident with the flexure seal diameter resulted in considerably lower leakage. System leakage was cut in-half with the E-seal build and cut by about 29 percent with the monofilament trial seal build.
- Using the trial seal positioned such that air pressure was exerted over greater back-side face-seal surface area decreased seal leakage sensitivity to carrier position—a desired result. Photographic evidence showed that the face seal contact shifted toward its inner diameter.
- Finite element analyses showed that at high (120 psig) air pressures the face seal contact pressure for the baseline design was greatest at its outer diameter—consistent with both the pressure sensitive film observations and original scuffing marks observed on the seal carriers.
- Analyses showed the benefit of moving the face seal balance diameter inward to increase face-seal back-side pressure loading and to more uniformly distribute load across the face seal under both inward and outward carrier motion, minimizing face seal edge loading. This result was corroborated by the leakage flow measurements.
- Analyses also showed the benefit of a thinner face seal and inward positioned E-seal. A 0.25 in. thick face seal exhibited more uniform contact pressure load across the face seal under both inward and outward carrier motion, minimizing face seal edge loading.

References

[1] Halila, E.E., Lenahan, D.T., Thomas, T.T., "Energy Efficient Engine, High Pressure Turbine Test Hardware Detailed Design Report," NASA CR–167955, 1982.

[2] Lattime, S.L., Steinetz, B.M., "Turbine Engine Clearance Control Systems: Current Practices and Future Directions," Journal of Propulsion and Power, vol. 20, no. 2, NASA/TM—2002-211794, also AIAA–2002–3790, presented at the AIAA/ASME/SAE/ASEE conference, July, 2002, Indianapolis, IN.

[3] Kawecki, E.J., "Thermal Response Turbine Shroud Study," Air Force Aero Propulsion Laboratory Technical Report AFAPL–TR–79–2087, 1979.

[4] Melcher, K.J., and Kypuros, J.A., "Toward a Fast-Response Active Turbine Tip Clearance Control," Proceedings of the XVI International Symposium on Air Breathing Engines, Cleveland, OH, August 31–September 5, 2003.

[5] DeCastro, J.A., Melcher, K.M., "A Study on the Requirements for Fast Active Turbine Tip Clearance Control Systems," Proceedings of the 40th Joint Propulsion Conference and Exhibit, AIAA–2004–4176, 2004.

[6] Lattime, S.L., Steinetz, Bruce M., Robbie, M., "Test Rig for Evaluating Active Turbine Blade Tip Clearance Control Concepts," NASA/TM—2003-212533, also AIAA–2003–4700, presented at the AIAA/ASME/SAE/ASEE conference, July, 2003, Huntsville, AL. *Journal of Propulsion and Power*, vol. 21 (3) May-June 2005.

[7] Steinetz, B.M., Lattime, S.B., Taylor, S., DeCastro, J.A., Oswald, J., Melcher, K.A., "Evaluation of an Active Clearance Control System Concept," NASA/TM—2005-213856, AIAA–2005–3989. Presented at the 2005 AIAA/ASME/SAE/ASEE Joint Propulsion Conference, Tucson, AZ.

[8] General Electric Aircraft Engines, "HPT Clearance Control (Intelligent Engine Systems)—Phase I—Final Report" NASA Contract NAS3–01135, April 2004.

[9] Wiseman, M.W., Guo, T., "An Investigation of Life Extending Control Techniques for Gas Turbine Engines," Proceedings of the American Control Conference, IEEE Service Center, Piscataway, NJ, IEEE Catalog No. 01CH37148, vol. 5, pp. 3706–3707, 2001.

[10] Shapiro, Ascher H., The Dynamics and Thermodynamics of Compressible Flow, The Ronald Press Co., New York, 1953.

REPORT DOCUMENTATION PAGE

Form Approved
OMB No. 0704-0188

1. AGENCY USE ONLY (*Leave blank*)	2. REPORT DATE	3. REPORT TYPE AND DATES COVERED
	February 2006	Technical Memorandum

4. TITLE AND SUBTITLE

Seal Investigations of an Active Clearance Control System Concept

5. FUNDING NUMBERS

WBS–22–714–92–56

6. AUTHOR(S)

Bruce M. Steinetz, Shawn Taylor, Jay Oswald, and Jonathan A. DeCastro

7. PERFORMING ORGANIZATION NAME(S) AND ADDRESS(ES)

National Aeronautics and Space Administration
John H. Glenn Research Center at Lewis Field
Cleveland, Ohio 44135–3191

8. PERFORMING ORGANIZATION REPORT NUMBER

E–15372–1

9. SPONSORING/MONITORING AGENCY NAME(S) AND ADDRESS(ES)

National Aeronautics and Space Administration
Washington, DC 20546–0001

10. SPONSORING/MONITORING AGENCY REPORT NUMBER

NASA TM—2006-214114

11. SUPPLEMENTARY NOTES

Prepared for the 11th International Symposium on Transport Phenomena and Dynamics of Rotating Machinery sponsored by the Pacific Center of Thermal Fluids Engineering, Honolulu, Hawaii, February 26–March 2, 2006. Bruce M. Steinetz, NASA Glenn Research Center; Shawn Taylor, University of Toledo, 2801 W. Bancroft Street, Toledo, Ohio 43606; Jay Oswald, J&J Technical Solutions, 14880 Timberlane, Cleveland, Ohio 44130; and Jonathan A. DeCastro, QSS Group, Inc., 21000 Brookpark Road, Cleveland, Ohio 44135. Responsible person, Bruce M. Steinetz, organization code RXM, 216–433–3302.

12a. DISTRIBUTION/AVAILABILITY STATEMENT

Unclassified - Unlimited
Subject Category: 37

Available electronically at http://gltrs.grc.nasa.gov

This publication is available from the NASA Center for AeroSpace Information, 301–621–0390.

12b. DISTRIBUTION CODE

13. ABSTRACT ***(Maximum 200 words)***

In an effort to improve upon current thermal active clearance control methods, a first generation, fast-acting mechanically actuated, active clearance control system has been designed and installed into a non-rotating test rig. In order to harvest the benefit of tighter blade tip clearances, low-leakage seals are required for the actuated carrier segments of the seal shroud to prevent excessive leakage of compressor discharge (P3) cooling air. The test rig was designed and fabricated to facilitate the evaluation of these types of seals, identify seal leakage sources, and test other active clearance control system concepts. The objective of this paper is to present both experimental and analytical investigations into the nature of the face-seal to seal-carrier interface. Finite element analyses were used to examine face seal contact pressures and edge-loading under multiple loading conditions, varied E-seal positions and two new face seal heights. The analyses indicated that moving the E-seal inward radially and reducing face seal height would lead to more uniform contact conditions between the face seal and the carriers. Lab testing confirmed that moving the balance diameter inward radially caused a decrease in overall system leakage.

14. SUBJECT TERMS

Seal; Active clearance control; Design; Leakage; Flow; Actuator; Clearance sensor; Turbine; High pressure turbine; Turbine engine; Experiments; Analyses; Finite element

15. NUMBER OF PAGES

22

16. PRICE CODE

17. SECURITY CLASSIFICATION OF REPORT	18. SECURITY CLASSIFICATION OF THIS PAGE	19. SECURITY CLASSIFICATION OF ABSTRACT	20. LIMITATION OF ABSTRACT
Unclassified	Unclassified	Unclassified	